J. Fluid Mech. (1983), *vol.* 136, *pp.* 167–187
Printed in Great Britain

The formation of an intermediate layer by horizontal convection in a two-layered shear flow

By DAVID L. WILKINSON
University of New South Wales, Water Research Laboratory

AND IAN R. WOOD
University of Canterbury, Department of Civil Engineering

(Received 10 May 1982 and in revised form 14 May 1983)

When two layers of different densities flow in opposite directions over a sill, it is possible for a stagnation point to occur at the interface. Experiments show that the flow towards such a point causes mixing and the continuous formation of a layer of intermediate density. Flow of this type may occur at specific locations in a fjord where the entrance is constricted by a sill.

1. Introduction

In a recent review Sherman, Imberger & Corcos (1978) described the mechanisms of mixing that could lead to the production of layers in a stratified fluid. One of the mechanisms they identified was that of the Kelvin–Helmholtz instability which converts the kinetic energy of large-scale shear flows to smaller dissipative scales. Sherman *et al.* then used Turner's (1973) energy argument to show that these shear instabilities can only disperse an initial discontinuity to a moderate degree. They concluded that, because a relatively sharp interface is required for the growth of the instability, a mixing event that causes thickening of the interface will suppress further mixing until the interface has been sharpened by the action of a shear field. From this it appears that the mixing from shear-flow instabilities will be intermittent both in time and space. A similar statement can be made about other mixing mechanisms such as internal wave interaction (Turner 1973) and the growth of a perturbation on a single wave (McEwan & Robinson 1975). The purpose of this paper is to describe a mechanism in which continuous mixing can be sustained.

When two layers flow in opposite directions over a sill, a stagnation point can be established on the interface, and advection of fluid towards the stagnation point results in the growth of an intermediate layer. The experiments described in this paper are of this type, and, although the flow in the vicinity of the stagnation point was necessarily unsteady, the exterior flow field remained steady or quasi-steady.

The conditions required for this mechanism to be operable can arise in a variety of ways. The most obvious of these is a two-layer shear flow over a variable geometry such as the sill of a fjord or on a large scale the flow out of some straits. In both of these examples it is possible to have an upper light layer flowing seaward and a lower denser layer flowing in the opposite direction.

The growth rate of the intermediate layer is examined as are the factors affecting its geometry. Finally some naturally occurring flows are described in which this mechanism may be important.

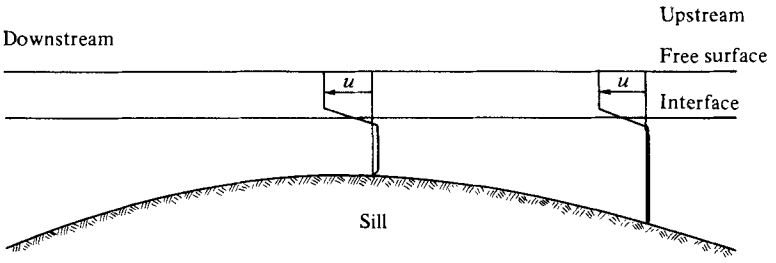

(*a*) Initial flow state—no net flow in lower layer

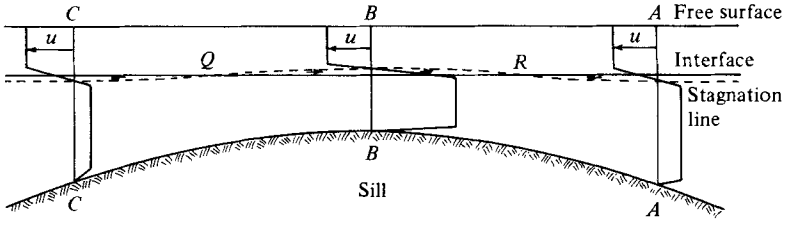

(*b*) Counterflow established in the lower layer

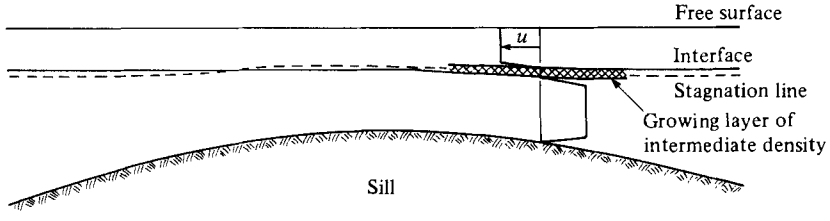

(*c*) Formation of a third layer

FIGURE 1. Schematic diagram of the mechanism that leads to the formation of the intermediate layer.

2. Description of the mechanism

The mechanism is most simply described by considering a two-layer shear flow between two wide reservoirs (figure 1*a*). The convention of describing upstream and downstream with respect to the upper layer will be adopted. Consider the case where there is a sharp non-diffusive interface. Let there be an established flow in the upper, less dense layer. This flow will, by viscous or turbulent drag, cause the upper portions of the lower layer to flow in the same direction as the upper layer and force a slow return flow deeper in the lower layer. If at some later time the lower layer is driven in the opposite direction, a two-layered shear flow will be established over the sill as shown in figure 1 (*b*). At sections such as AA where the lower layer is deep, the velocity will be much less than that in the upper layer. This implies that in this region some of the lower layer will still be dragged along with the upper layer.

A similar statement can be made about section CC. However, at section BB where the geometry forces the velocity in the lower layer to exceed that in the upper layer, the reverse is true and some of the upper layer will be dragged in the direction of the flow in the lower layer. Thus the velocities on the interface at sections AA and CC and that at BB are in opposite directions and two stagnation points R and Q must exist on the interface. Between BB and CC fluid at the interface is advected away from the stagnation point Q, and between AA and BB fluid at the interface is advected towards the stagnation point R.

The description of the flow field given above is both idealized and can only last for an instant of time since once the stagnation point between AA and BB is established it leads to an accumulation of fluid in this region. In real fluids, where the density gradient is continuous across the interface, this flow field produces an accumulation of interfacial fluid at the stagnation point, and the formation of a third layer of intermediate density. The flow changes rapidly to that shown in figure 1 (*c*).

Although, in the experiments to be described, a sill was used to produce a convergent flow towards a singularity within a stratified shear layer, it is unlikely that this is the only geometry in which the mechanism may operate.

3. Experimental apparatus and technique

An experimental facility was designed to simulate the flow over the sill as described in §2. The layout of the facility is shown in figures 2 and 3. A tilting tank 5 m long, 250 mm high and 250 mm wide was fitted with a working section 80 mm wide and 1.5 m long. The working section, which occupied only one-third of the total tank width, was installed to minimize end effects and also to reduce shear velocities over much of the tank. Bulkheads were fixed behind the false wall of the working section to keep the area behind the working section free of fluid. This enabled the use of the shadowgraph technique in the working section. A sill of parabolic profile 1 m long and 82 mm high was installed in the working section.

Flow in the lower layer was recirculated, and a valve and rotameter were employed to set and meter the flow rate. The lighter upper layer was not recirculated but was pumped from a storage tank via a flow-control valve and a rotameter into the flume. It was then discharged freely to waste over a sharp crest weir located in the tank. The upper and lower layers entered the tank through plastic-foam filters. Injection of dye into the flow showed that the filters produced very uniform and non-turbulent flows across the full width of the tank. The head loss across the filters was approximately 50 mm at the design flow rate.

The vertical distance between the crest of the sill and the weir was 72 mm, and at the commencement of an experiment the thickness of the upper layer was typically 40 mm while that of the lower was about 35 mm at the crest of the sill. Typical flow rates in both layers were of the order of 0.1 L s^{-1} producing velocities in the working section of up to 40 mm s^{-1}, while outside the working section the velocity in the upper layer was typically of the order of 10 mm s^{-1} and that in the lower layer only 4 mm s^{-1}. The higher velocity in the upper layer outside of the working section caused an accumulation of diffuse interfacial fluid at the overflow weir (at A in figure 2). A wedge-shaped region of intermediate density slowly grew back from the weir towards the working section. However, under typical experimental conditions it took some 20 min before this trapped wedge intruded into the working section, and as experiments lasted less than 5 min the trapped wedge did not affect flow in the working section in any way.

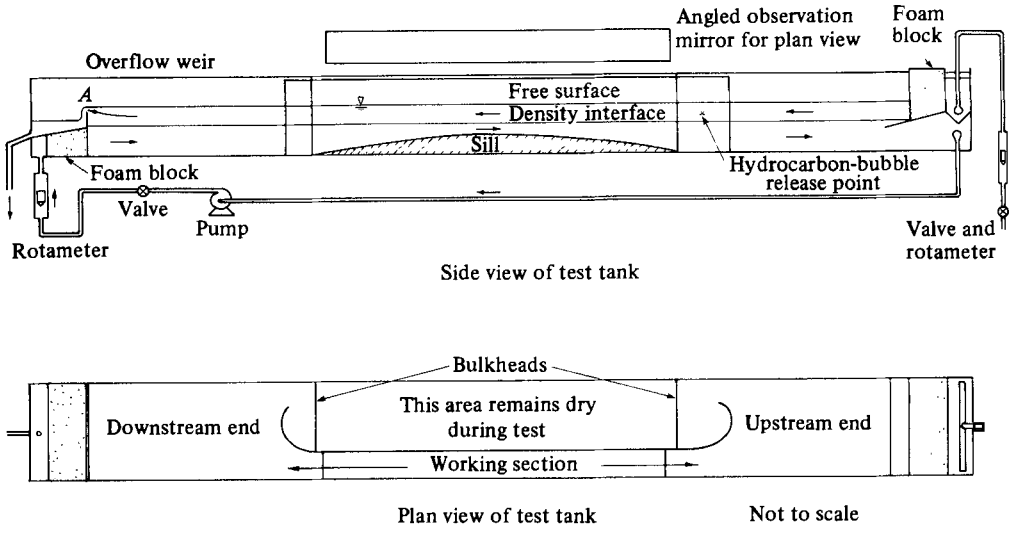

FIGURE 2. Schematic diagram of the test facility.

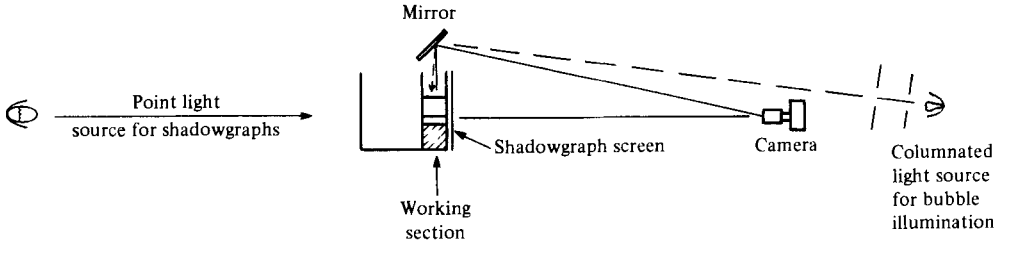

FIGURE 3. Cross-section of the test facility illustrating the photographic technique.

The flow rate was initially set at approximately 0.03 L s^{-1}, and the light layer floated over the denser layer with no discernible interfacial mixing or disturbances visible anywhere on the interface. When the surface layer was approximately 10 mm deep the flow in the upper layer was increased to the final experimental value of about 0.1 L s^{-1} and the tank filled until a steady overflow drained from the left-hand end of the tank. At no stage during the filling process were disturbances visible at the interface. Steady flow conditions were achieved about 10 min after the lighter fluid was first introduced to the tank.

The halocline thickness in the working section was typically 2–3 mm, while the depth of the sheared region was approximately 15 mm. The density difference between the layers was such that the interfacial flow was stable and non-turbulent.

Various visualization techniques were employed to determine the structure of the flow (figure 3), and shadowgraph was used extensively to observe the growth of the intermediate layer.

Two techniques were employed to measure velocities within the flow. Vertical distributions of the horizontal velocity component were obtained at a number of sections using the hydrogen-bubble technique. Neutrally buoyant tracer bubbles were also used to study the flow field. A device was constructed which injected small bubbles (1–2 mm in diameter) of a mixture of carbon tetrachloride, xylene and

oil-based white paint into the flow. These bubbles had a density between the densities of the upper and lower layers and therefore resided at the interface of the two layers after release. The bubbles were coloured a brilliant white and, by use of a mirror, were photographed in plan against the black bottom of the working section to produce a streak on a 5 s time exposure. The alignments of the camera and the mirror are shown in figure 3. The camera lens was covered for one second after the initial second of exposure before exposing for a further 3 s. The short and long dash registered on the photograph enabled the direction of the flow on the interface to be identified. The intensity of the shadowgraph back lighting was adjusted so that the exposure settings for both the bubble streaks and the shadowgraph image were the same. This enabled the vertical structure to be recorded simultaneously with the interfacial velocity field on the one photograph.

It would have been highly desirable to have taken density profiles through the intermediate layer during its development. However, the short duration of the experiments (less than 5 min) combined with the rapid growth of the layer made profiling impractical. The complex lighting and photographic requirements also limited access to the working section during an experimental run. Instead, single Moiré screens were used to gain a qualitative impression of density gradients within the intermediate layer (figures 5 and 8). The intensity of density gradients can be assessed by the distortion of the pattern of diagonal lines on the Moiré screen when it is viewed through the fluid. Neutrally buoyant hydrocarbon bubbles were also used as density indicators within the intermediate layer.

4. Development of the intermediate layer

The sequence of photographs in figure 4 follows the development of the intermediate layer in a typical experiment. Scaling of these experiments will be discussed later in §5; however, in the experiment shown in figure 4, velocities in both layers were an order of magnitude less than the celerity of a long interfacial wave.

Figure 4 (*a*) shows the initial flow state with flow only in the upper layer. The lowest photograph is a side-view shadowgraph of the tank. The photograph immediately above is a simultaneous plan view of the tank and shows a line of white dots along the centreline of the working section. These dots are white hydrocarbon bubbles floating at the interface between the layers. The topmost photograph shows a 5 s time exposure of the bubbles. The time exposure was taken immediately after the instantaneous exposures shown in the two photographs below. The plan views were obtained using an angled mirror sited above the working section as shown in figure 3.

Lengthscales in the experiment can be gauged from the rectangular grid marked on the side of the test tank and is clearly visible in the shadowgraph images. The grid lines are at horizontal and vertical spacings of 100 mm and 25 mm respectively.

The interface in figure 4 (*a*) is the heavy nearly horizontal line located 36 mm above the crest of the sill. The free surface is the next heavy line above and is located 73 mm above the crest, giving an upper-layer depth of 37 mm. The direction and magnitude of the velocities at the interface can be obtained from the time exposure shown in the upper plan view of the working section. The shorter dashes give the initial position of the hydrocarbon bubbles while the end of the long dash gives the bubble position 5 s later. At the stage of the experiment shown in figure 4 (*a*) the mean velocity of the upper layer in the working section of the tank was 22 mm s^{-1} and the velocity indicated by the bubble streaks was 13 mm s^{-1}. The halocline was very thin, and at

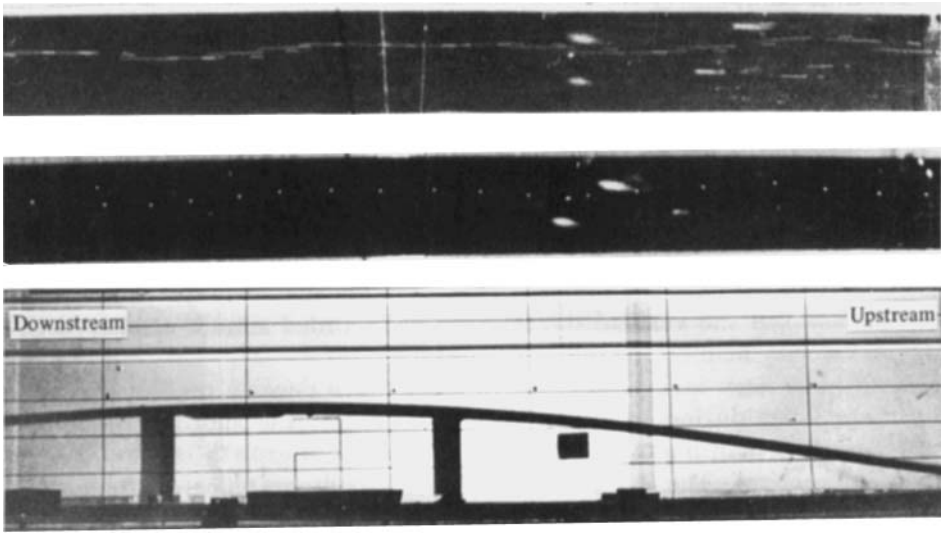

(*a*)

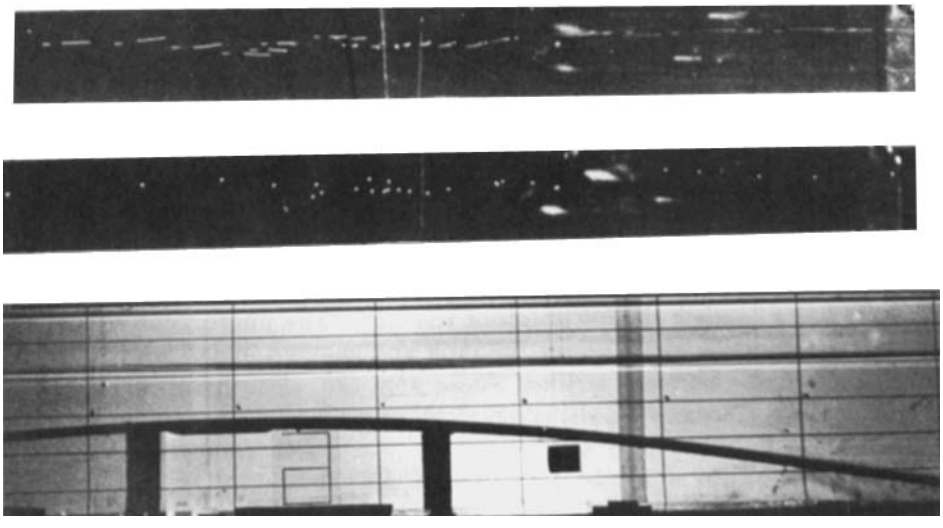

(*b*)

FIGURE 4. For caption see facing page.

this stage velocities at the interface were everywhere in the direction of flow of the upper layer.

At the commencement of flow in the lower layer, the initial response was barotropic, which above the sill produced a flow reversal over the entire depth, with the fluid behaving as though it were homogeneous. Thus there was a rapid adjustment of free-surface levels either side of the working section followed by a slower adjustment of the internal flow. The surface adjustment took approximately 5–10 s, while the internal flow took approximately a minute to become fully established.

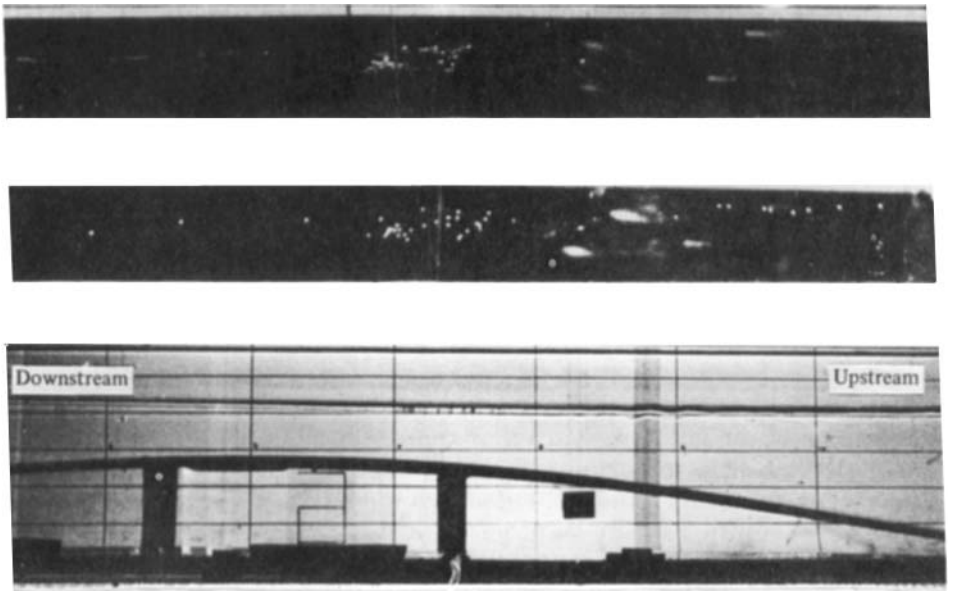

(*c*)

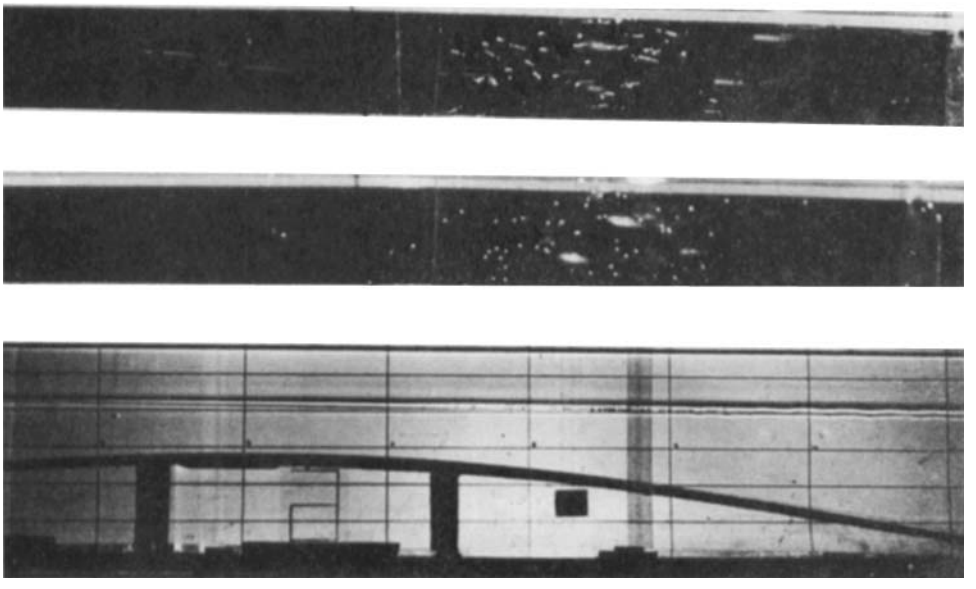

(*d*)

FIGURE 4. Development of an intermediate layer in highly stratified two-layer flow (experiment no. 6; $\Sigma F^2 = 0.09$, $Ri = 14.7$, $Re = 350$). (*a*) $t = -10$ s ($\xi t = -12$); initial conditions with flow from left to right in the upper layer only. (*b*) $t = 26$ s ($\xi t = 32$); counterflow commenced in lower layer, producing a flow reversal at the interface in the vicinity of the sill crest. The intermediate layer has begun to form as evidenced by the accumulation of hydrocarbon bubbles. However, the intermediate layer is not yet visible in the shadowgraph. (*c*) $t = 60$ s ($\xi t = 73$); continued growth of the intermediate layer, which is now visible in the shadowgraph and is bounded by distinct upper and lower interfaces. The uppermost plan view (a time exposure of 5 s duration) shows continued flow into the intermediate layer and accumulation of bubbles within the layer. (*d*) $t = 118$ s ($\xi t = 129$); flow into the intermediate layer continues. Note the increased thickness of the layer.

Figure 4(*b*) shows the situation 26 s after commencement of the counterflow in the lower layer. Disturbances were just starting to appear on the interface and there was a clearly convergent flow in the halocline with opposed velocities either side of the stagnation region. Hydrocarbon bubbles can be seen accumulating in the plan view of this area.

The intermediate layer is clearly visible in figure 4(*c*), which was taken 60 s after the commencement of flow in the lower layer. Shadows of hydrocarbon bubbles which had accumulated in the intermediate layer are now visible in the shadowgraph in figure 4(*c*). The plan-view time exposure shows that interfacial fluid continued to flow towards the intermediate layer from both directions.

Figure 4(*d*), taken after 118 s, shows further thickening of the intermediate layer, which now extended well to either side of the sill. Loss of fluid from the layer was occurring on the downstream (left-hand) side of the sill because the layer extended past the region of the initial second stagnation point (*Q* in figure 1*b*). Downstream of *Q* the higher velocities in the upper layer caused interfacial fluid to flow away from the sill in the downstream direction. Growth of the intermediate layer was reduced, and ultimately a limiting steady-state condition was established where flow into the intermediate layer on the upstream side was balanced by a corresponding drainage from the layer on the downstream side. This steady-state condition was not investigated in detail owing to the limited length of the working section in this study.

A more detailed view of the intermediate layer is shown in figure 5. The stratification in this experiment (no. 7) was weaker than was the case for the experiment shown in figure 4 (see table 1 for details). A section of the shadowgraph screen was removed to show a Moiré screen attached to the far side of the working section. Curvature of the diagonal lines on the Moiré screen indicates the presence of density gradients, and inspection of the screen in this photograph reveals a smooth distortion of the lines at the upper halocline. The halocline is also clearly visible in the adjacent shadowgraphs.

The continuity of the Moiré lines indicates that the flow in the region of the halocline is non-turbulent. Within the intermediate layer, irregular distortion of the lines points to the presence of turbulence, although the orientation of the lines in the central region of the layer (where the lines are roughly parallel to those above and below the intermediate layer) indicates an absence of steep density gradients within that region of the layer. The lower interface is also clearly visible; however, curvature of the Moiré lines is less than that at the upper interface, revealing that the density jump across it is also less.

These observations suggest that the density of the intermediate layer is closer to that of the lower flowing layer than of the upper flowing layer. This was confirmed by withdrawal of a fluid sample from the intermediate layer. Measurement of the salinity of the sample taken in this experiment showed the intermediate layer to be composed of one part fluid derived from the upper layer to three parts fluid derived from the lower layer. The factors which affect the composition of the intermediate layer are now examined.

Figure 6 shows what the authors believe to be the streamline pattern associated with the development of the intermediate layer. This conception is based on flow visualizations using dye probes and neutrally buoyant markers in addition to photographic records. For clarity, the vertical scale in this figure has been exaggerated.

The original interface, before development of the intermediate layer, would have coincided with the streamlines labelled *C* and *B*, which subsequently divided to form

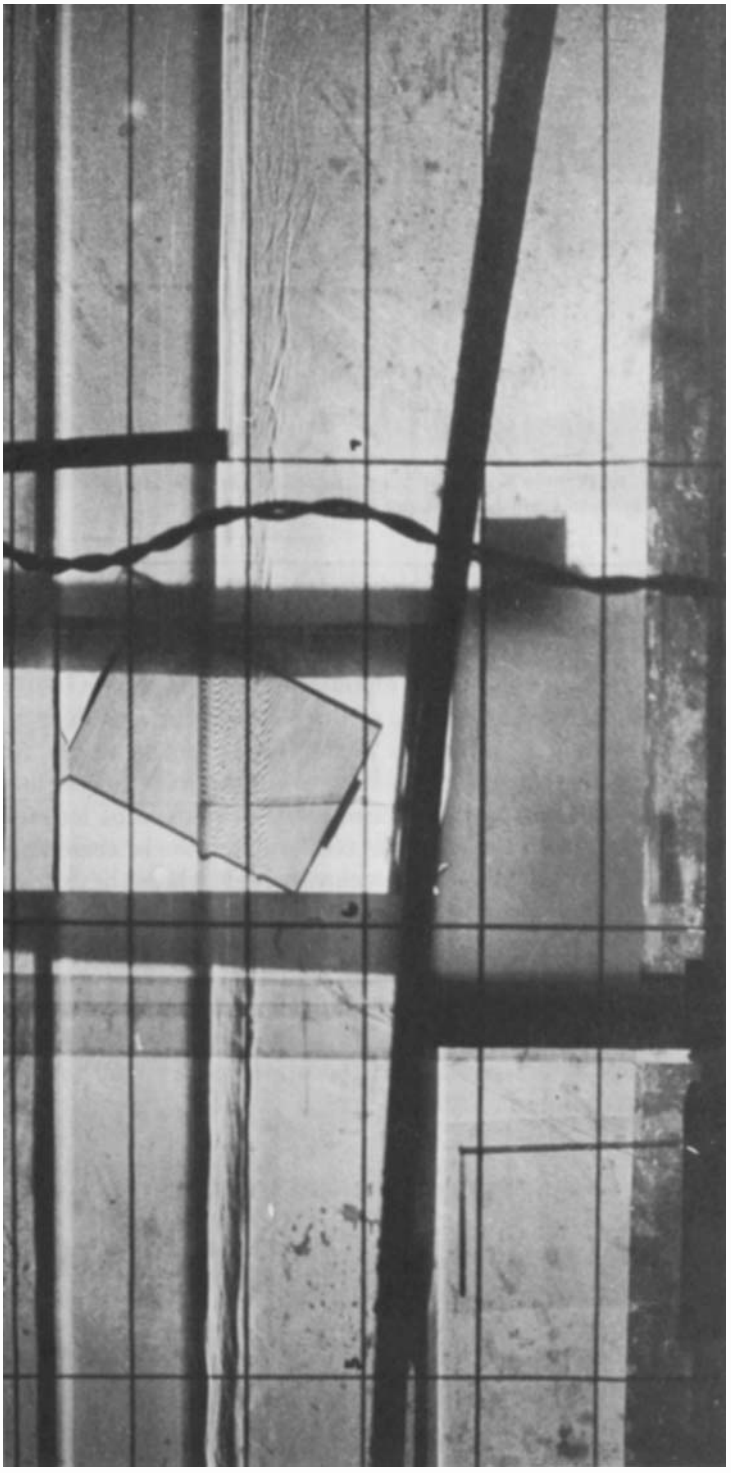

FIGURE 5. A close-up view of the intermediate layer in experiment no. 7 at dimensionless time $\xi t = 161$. The Moiré screen viewed through the fluid in the centre of the photograph indicates the presence of three relatively homogeneous layers separated by upper and lower density interfaces. Shadowgraph images can be seen to either side of the screen. That on the left shows the intermediate layer confined between strong interfaces, while that on the right shows the upstream end of the intermediate layer and the wake region beyond.

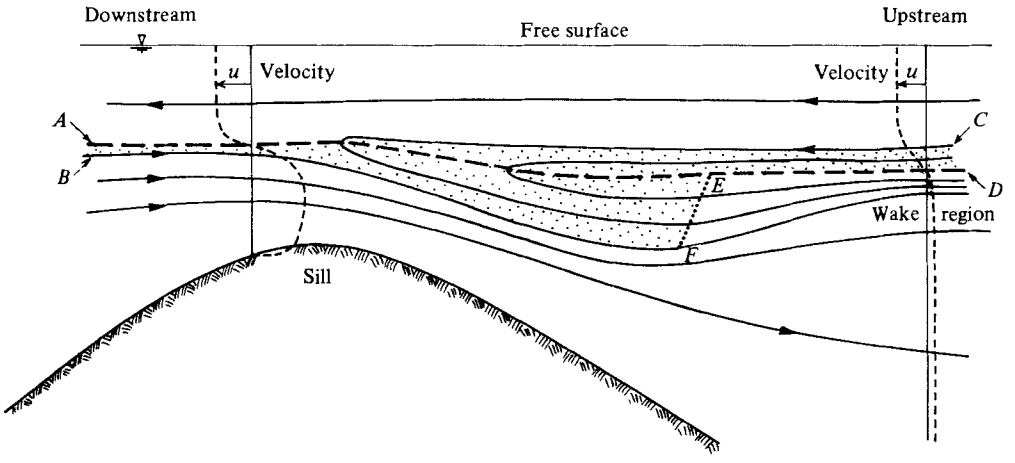

FIGURE 6. The flow pattern associated with the development of the intermediate layer. The intermediate layer is identified by cross-hatching.

the upper and lower boundaries of the intermediate layer. Flow into the intermediate layer from the upstream side is derived from the shear layer between the dividing streamline C and the stagnation line D (the latter is shown as the dashed curve in figure 6). Similarly, on the downstream side, inflow to the intermediate layer comes from the shear layer between A and B. Mixing of the highly rotational fluid entering the intermediate layer causes it to be relatively homogeneous and separated from the adjacent flowing layers by sharp interfaces. As the area of the mixed layer increases, its upstream limit EF advances upstream. Because the development length of the shear layer is much greater on the upstream side, the flow into the intermediate layer from this side greatly exceeded that from the downstream side where the development length of the shear layer between streamlines A and B is restricted to the region of the sill crest. As flow into the intermediate layer from the upstream side (between streamlines C and D in figure 6) lies predominantly below the interface while the flow entering from the upstream side (between streamlines A and B) lies predominantly above the interface, it follows that the density of the intermediate layer would be closer to that of the bottom layer rather than the upper layer. This conclusion is supported by the experimental observations.

5. The hydraulics of the flow and the scaling and growth of the intermediate layer

It follows from the description of intermediate layer development in §4 that the growth and shape of the intermediate layer is affected by two independent factors. The first is the nature of the stratified shear layer on the upstream side of the sill from which most of the fluid comprising the intermediate layer is derived. The second factor relates to the internal hydraulics of the flowing layers above and below the intermediate layer. Fluid in the intermediate layer was almost stationary, so that it acted very much like an internal manometer. The interfaces which formed the upper and lower boundaries of the intermediate layer therefore reflected the piezometric levels of the flowing layers. Thus the shape of the intermediate layer was largely determined by the internal hydraulics of the flowing layers. However, the initial growth rate of the intermediate layer was found to be quite insensitive to densimetric

effects. The hydraulics of the flow will be discussed first, and this will be followed by a discussion of the parameters which affect the growth of the intermediate layer.

The hydraulics of the upper and lower layers can be described in terms of three Froude numbers

$$F_0 = \frac{U_u}{[g(h_\ell + h_u)]^{\frac{1}{2}}}$$

(a Froude number characterizing the barotropic nature of the flow),

$$F_u = \frac{U_u}{(g' h_u)^{\frac{1}{2}}}, \quad F_\ell = \frac{U_\ell}{(g' h_\ell)^{\frac{1}{2}}},$$

where F_u and F_ℓ are densimetric Froude numbers characterizing the internal flows in the upper and lower layers respectively.

The depths and velocities of the upper and lower layer (h_u and h_ℓ and U_u and U_ℓ respectively) were measured at the crest of the sill after commencement of the counterflow.

The reduced gravity g' is given by

$$g' = (\rho_\ell - \rho_u)\frac{2g}{\rho_u + \rho_\ell},$$

where ρ_u and ρ_ℓ are the densities of the upper and lower layers respectively and g is the gravitational acceleration.

The barotropic and internal flows were subcritical at the commencement of all the experiments so that the sill did not act as a control. The internal flow above the sill remained subcritical so long as

$$\Sigma F^2 = F_u^2 + F_\ell^2$$

was less than unity.

The parameters that affect the growth of the intermediate layer will now be examined. Prior to the establishment of the flow in the lower layer, the characteristics of the interfacial shear layer (its thickness and rate of shear) are determined by the mean velocity in the upper layer U_u, the length L available for the development of the shear layer, the boundary geometry of the flow, and the diffusivities of vorticity ν and solute D. The time for development of the shear layer is then

$$t_0 \sim \frac{L}{U_u},$$

and the characteristic thickness and rate of shear are respectively

$$\delta \sim (\nu t_0)^{\frac{1}{2}},$$

$$\xi \sim \frac{U_u}{\delta} \sim \frac{U_u^{\frac{3}{2}}}{(\nu L)^{\frac{1}{2}}}.$$

The non-dimensional parameters which then determine the nature of the upstream stratified shear layer for this geometry are

$$Re = \frac{U_u \delta}{\nu} \quad \text{(a Reynolds number)},$$

$$Sc = \frac{\nu}{D} \quad \text{(a Schmidt number)},$$

$$Ri = \frac{g' \delta}{U_u^2} \quad \text{(a Richardson number)}.$$

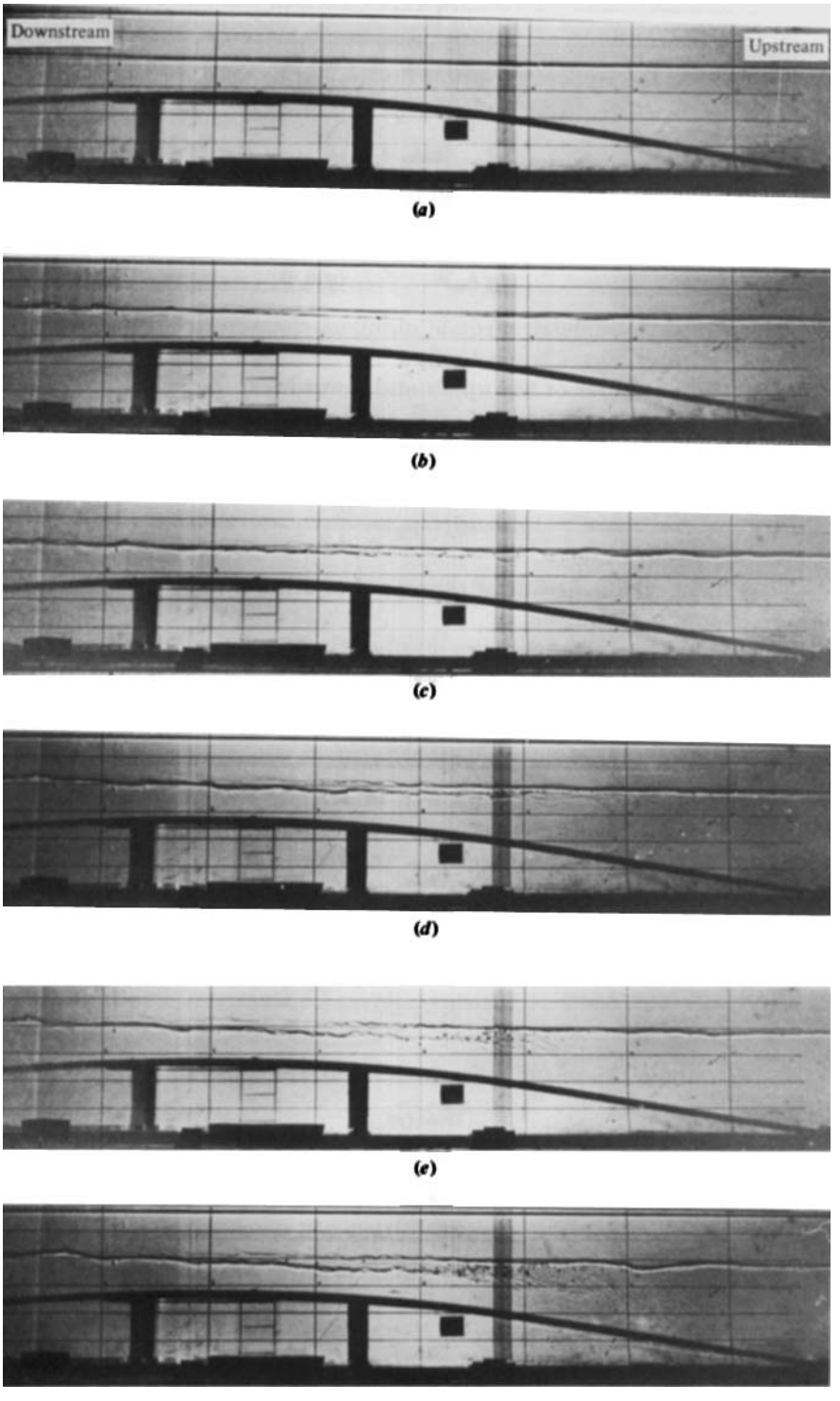

FIGURE 7. For caption see facing page.

Magnitudes of the experimental variables

Experiment no.	Values at the sill crest U_u (cm s^{-1})	U_ℓ (cm s^{-1})	h_u (cm)	h_ℓ (cm)	g' (cm s^{-2})	δ (cm)	ξ (s^{-1})	t_0 (s)
6	2.17	2.75	3.7	3.6	39	1.77	1.23	290
7	2.78	3.56	4.0	3.4	40	1.57	1.77	220
8	2.71	4.12	4.1	3.3	20	1.59	1.70	230
9	3.09	3.78	3.6	3.8	10	1.49	2.07	200

Experiment no.	Figure no.	ΣF^2	F_0	F_u	F_ℓ	Re	Sc	$\frac{U_\ell}{U_u}$	Ri
6	4	0.09	0.034	0.18	0.23	350	1010	1.27	14.7
7	5	0.15	0.044	0.22	0.31	400	1025	1.29	8.0
8	7	0.35	0.043	0.30	0.51	390	1015	1.52	4.2
9	10	0.61	0.052	0.51	0.58	420	1010	1.16	1.53

TABLE 1

Once the flow commences in the lower layer, two further parameters are introduced. They are the velocity in the lower layer and the time t since the start of the lower-layer flow. This implies that there are two further dimensionless parameters necessary to define the properties of the stratified shear layer. These are U_ℓ/U_u and ξt. In the experiments that were designed to demonstrate the mixing mechanism the values of the Reynolds and Schmidt numbers were not varied significantly (table 1).

Further, as already discussed, the value of U_ℓ/U_u determines the initial positions of the stagnation points, and to maintain these close to the crest the variation in this parameter was limited (table 1). The velocity in the upper layer in regions away from the sill was appreciably greater than that of the lower layer because of the depth of this layer. Thus the velocity of the upper layer was the more significant velocity as regards development of the shear layer upstream of the stagnation point. Consequently a time scale based on ξ is adequate to describe the growth of the intermediate layer. It can be seen from table 1 that the experiments covered a wide range of inertial buoyancy conditions (Ri) and that the interfacial shear layer remained laminar ($Ri > 1$).

The remaining experiments will now be described in terms of the above non-dimensional parameters. In the next experiment, shown in figure 7, the density difference between the layers was reduced to 0.020 g/cm^3, increasing ΣF^2 to 0.35 compared with $\Sigma F^2 = 0.09$ in previous experiment (no. 6). Only the shadowgraph

FIGURE 7. Development of an intermediate layer in moderately stratified two-layer flow (experiment no. 8; $\Sigma F^2 = 0.35$, $Ri = 4.2$, $Re = 390$). (*a*) $\xi t = 56$; slight drawdown of the interface can be seen, although the intermediate layer is not yet visible on the shadowgraph. (*b*) $\xi t = 83$; interface has divided to form an intermediate layer. (*c*) $\xi t = 106$; intermediate layer has extended in the vertical and horizontal directions. (*d*) $\xi t = 235$; growth rate of the mixed layer has reduced. (*e*) $\xi t = 402$; wake region clearly visible on the left-hand side of the intermediate layer. (*f*) $\xi t = 847$; the mixed layer has reached a steady state. Inflow from the shear layer is balanced by fluid loss into the wake.

images are shown in figure 7 as the plan views were similar to those already shown in figure 4.

A cursory comparison of the shape of the intermediate layer in figures 4 and 7 reveals a marked change in the shape of the layer. The reduction in buoyancy has produced an appreciable increase in the thickness of the intermediate layer relative to its length. This feature is investigated more fully later in this section.

The first photograph (figure 7*a*) shows the flow at dimensionless time $\xi t = 56$. Some drawdown is visible on the interface above the sill, and interfacial disturbances can also be seen in the same region. Figure 7(*b*), taken at $\xi t = 83$, shows a clear division of the interface with a definite intermediate layer starting to form. The intensity of wave-like disturbances at the interface has increased. In figures 7(*c*, *d*, *e*), taken at $\xi t = 106$, 235, 402, the area of the intermediate layer has continued to increase, as has the intensity of the turbulence within the intermediate layer as vorticity continues to accumulate from the adjacent shear layers.

Turbulent wake-like regions were detected at either end of the intermediate layer. Wisps of fluid from the intermediate layer were entrained into these wake regions and were swept away in a lower layer. The rate of fluid loss from the intermediate layer into the wakes increased as the depth of the layer increased, thereby reducing and ultimately limiting the growth of the intermediate layer. These wake regions are visible in figure 7. For example at time $\xi t = 402$ (figure 7*e*) the intermediate layer extends as far as the third vertical grid line from the right-hand side. To the left of this grid line, distinct upper and lower interfaces are visible, indicating the presence of fluid of intermediate density between them. Further to the right, however, only the upper interface persists, indicating that the fluid below the interface is relatively homogeneous. Although turbulent mixing of wisps entrained from the intermediate layer render the wake visible in the shadowgraph, the density of this region is not measurably different to that of the lower layer. Further evidence of this is shown in figure 8, which shows a Moiré screen viewed through the wake. The lack of distortion in the screen image, except in the immediate vicinity of the interface, points to the homogeneity of the upper and lower layers in this region, in spite of the fact there was sufficient fluid escaping from the intermediate layer to register on the shadowgraph.

The hydrogen-bubble lines visible in figure 8 show a reasonably uniform velocity distribution in the upper layer, with strong shear in the region of the interface. Two zones can be identified from the bubble traces in the lower layer. In the wake, which extends from the interface to the second grid line below, the flow is turbulent and exhibits a relatively uniform mean shear. Below lies the main flow in the lower layer, and velocities here are appreciably greater than those in the wake above, while relative turbulence intensities are reduced. Figure 8 was taken under experimental conditions identical with those shown in figure 7(*e*) and at a section between the second and third vertical grid lines from the right-hand side of that figure.

The reduction of the density difference between the layers in experiment no. 8 produced a noticeable change in the shape of the intermediate layer compared with experiment no. 6. A shape parameter, the aspect ratio of the layer, is defined as the length l of the intermediate layer divided by its mean thickness A/l, where A is the area of the intermediate layer. The intermediate layer for the purposes of measuring l and A was taken as the region contained between distinct upper and lower interfaces as seen from the shadowgraph image. The presence of distinct interfaces indicated that the fluid contained between them was of different density to the flowing layers above and below. The area and length thus defined could be estimated with a

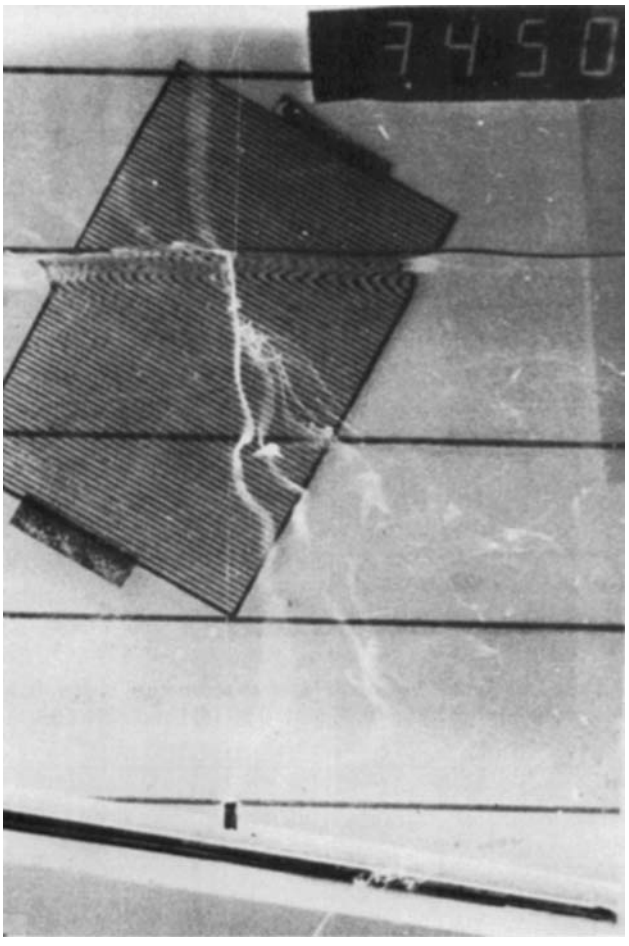

FIGURE 8. Velocity and density structure of the wake region as indicated by hydrogen-bubble lines and a Moiré screen respectively. The flow state is identical with that shown in figure 7(*e*). Note the relatively thin halocline upstream of the intermediate layer. The turbulent wake caused by the presence of the intermediate layer is clearly visible in the lower layer. The lack of distortion below the interface indicates that the lower layer is homogeneous.

consistency (variance ratio) of better than 15 %. The variance resulted from a degree of subjectivity in identifying the upstream and downstream limits of the intermediate layer. It should also be noted that when the density stratification was very strong (for example in experiment no. 6 shown in figure 4) the intermediate layer was extremely thin and its area could not be measured with acceptable accuracy.

The aspect ratio l^2/A of the intermediate layer is plotted in figure 9 as a function of the dimensionless time ξt.

Aspect ratios are shown for experiments 7, 8 and 9. In these experiments the buoyancy was varied considerably. It is apparent that the shape of the intermediate layer is very sensitive to buoyancy effects at values of ΣF^2 between 0.1 and 1 and responds to drawdown effects of the internal flow.

It can also be seen that the aspect ratio attains a maximum value and thereafter there is a relative thickening of the intermediate layer. This is associated with a change in the growth rate of the layer which occurs when it has grown to such a size that it begins to modify the surrounding flow field.

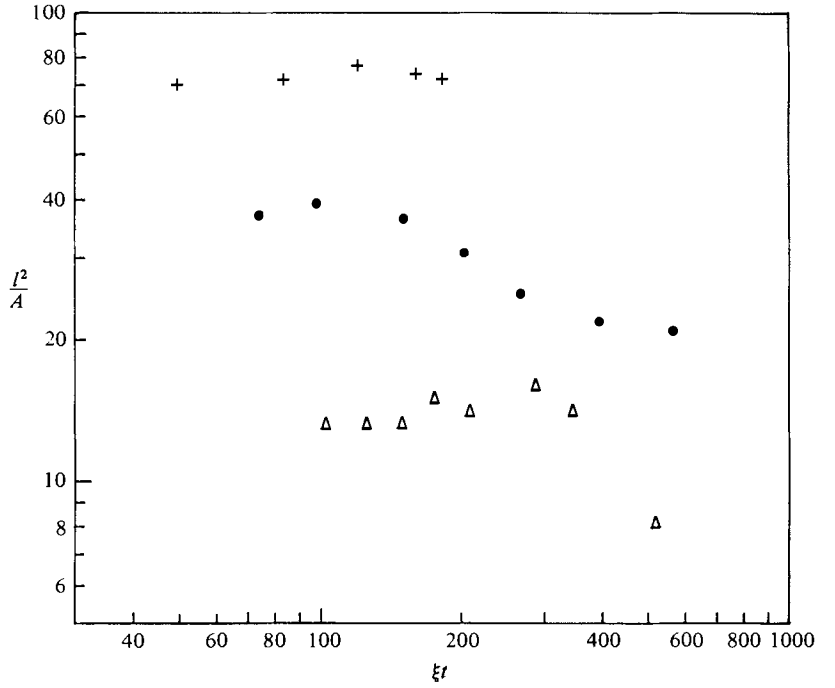

FIGURE 9. Aspect ratio of the intermediate layer as a function of the dimensionless time parameter for $\Sigma F^2 = 0.15$ (+), 0.35 (●) and 0.61 (△).

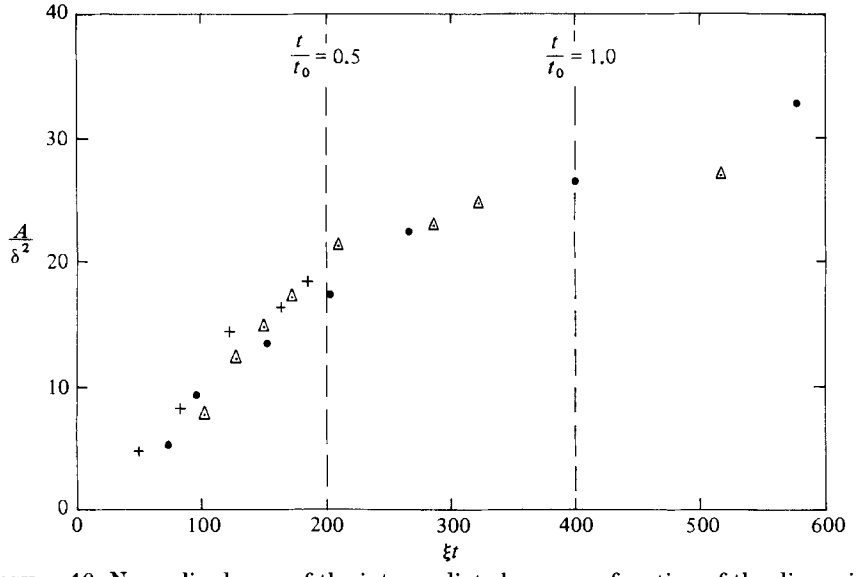

FIGURE 10. Normalized area of the intermediate layer as a function of the dimensionless time parameter for $\Sigma F^2 = 0.15$ (+), 0.35 (●) and 0.61 (△).

In view of the sensitivity of the shape of the intermediate layer to densimetric influence, it is remarkable that the initial growth rate of the layer appears to be quite insensitive to buoyancy effects. This can be seen in figure 10, where the growth of the intermediate layer is shown for experiments 7, 8 and 9. The areas of the intermediate layers were normalized by dividing by δ^2 and are plotted against the non-dimensional time ξt. Although the experiments covered a wide range of buoyancy

conditions ($\Sigma F^2 = 0.15$, 0.35 and 0.61) the normalized growth rates were similar. It should be noted that the normalizing parameters relate to the properties of the upstream shear layer and do not involve buoyancy.

These results suggest that the rate of growth of the intermediate layer is not sensitive to the internal hydraulics of the flowing layers but is determined by the nature of shear layer from which the intermediate layer is derived. For dimensionless time ξt less than 200 the normalized growth rate $\delta^{-2}\xi^{-1}\,\mathrm{d}A/\mathrm{d}t$ of the intermediate layer was found to be 0.092 ± 0.025. At times in excess of $\xi t = 200$ (which in these experiments corresponded to $t/t_0 \approx \frac{1}{2}$) the rate of intermediate-layer growth was observed to reduce. At this stage, the thickness of the intermediate-layer was a significant fraction of the depths of the flowing layers, so that baroclinic effects were beginning to modify the surrounding flow field. Also by time $t = \frac{1}{2}t_0$ the counterflow, although of much lower velocity than that of the upper layer, would have modified the velocity structure of the upstream shear layer.

The reduction in the growth rate of the intermediate layer was the result of fluid loss into the wakes at either end of the region. The loss rate increased as the area of the mixed layer increased, and ultimately the intermediate layer appeared to reach a state of equilibrium with no further growth. Because of the limited size of the available facility it was not possible to investigate the equilibrium state in detail.

It must be emphasized that the collapse of the data in figure 10 cannot be regarded as conclusive evidence that δ and ξ are the only variables affecting the growth rate of the intermediate layer as neither δ nor ξ was varied significantly in the different experiments.

In the final experiment to be described (no. 9) a new phenomenon was observed. At the start of the experiment the internal flow was close to critical with $\Sigma F^2 = 0.61$. The density difference between the layers was 0.010 g/cm^3, while the initial depths, velocities and flow rates were similar to those in the two experiments described previously. Once the intermediate layer formed the density difference between it and the lower layer was such that the flow in the lower layer became supercritical, causing an internal hydraulic jump to form beneath the intermediate layer. Fluid was entrained from the intermediate layer into the internal jump, to be convected away by the flow in the lower layer. As the entrainment by the jump exceeded the convective inflow into the intermediate layer, the area of this layer decreased. Ultimately the entire intermediate layer was engulfed in this manner.

The development of the intermediate layer and subsequent disappearance can be followed by the sequence of photographs shown in figure 11.

In the first photograph, taken at $\xi t = 102$, the interface is seen to divide to form upper and lower interfaces separated by an intermediate layer as occurred in the previous experiments. Shadows of hydrocarbon bubbles are visible on the interface and in the intermediate layer. At this stage, apart from its reduced aspect ratio, the intermediate layer is not noticeably different to that seen in the earlier experiments. The next photograph, taken at $\xi t = 150$, shows an upstream migration of the intermediate layer and the development of the wake-like regions at either end of the layer. The interface itself appeared more unstable, and weak breaking of interfacial waves was observed. Note also the marked depression of the lower interface beneath the intermediate layer; this is even more pronounced in the next photograph, taken at $\xi t = 210$. Flow in the lower layer was supercritical to the right of the crest in figure 11 (*d*), and a weak internal jump developed in the lower layer towards the right-hand end of the intermediate layer. Entrainment of fluid from the intermediate layer into the jump resulted in a reduction in the area of the intermediate layer. In the final

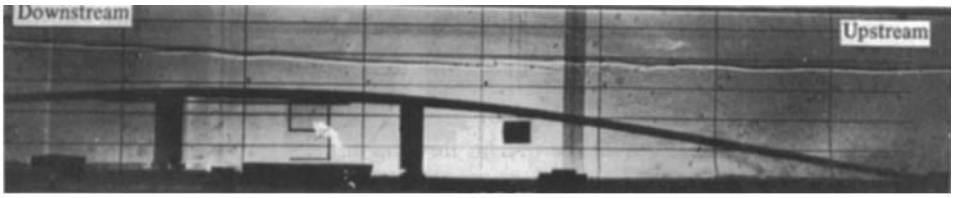

(a)

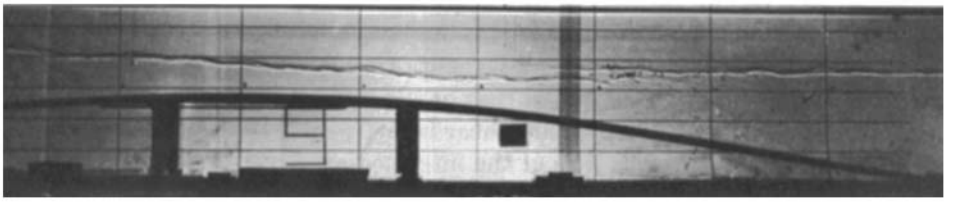

(b)

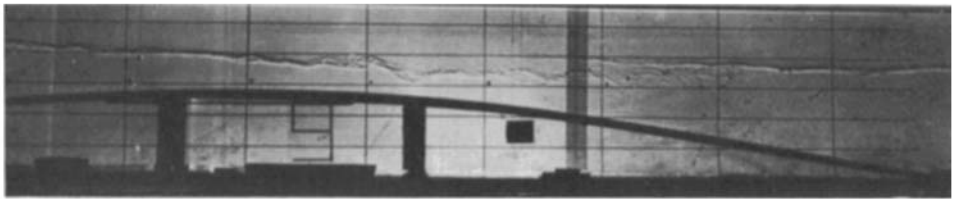

(c)

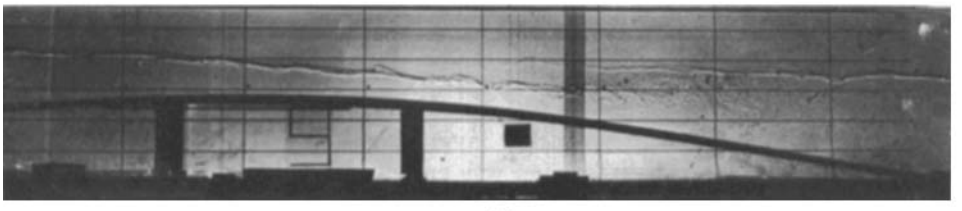

(d)

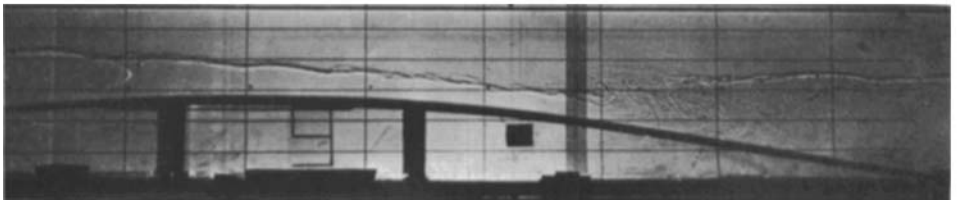

(e)

FIGURE 11. For caption see facing page.

photograph (figure 11 *e*) the intermediate layer has disappeared. An internal hydraulic jump is visible between the 2nd and 3rd grid lines from the right-hand side of the photograph.

The form of the internal jump with counterflowing layers is rather different to those described by Wilkinson & Wood (1971), where one of the layers was stagnant. In particular, the length of the mixing region was substantially reduced.

6. Discussion

The experiments have shown that the formation of a stagnation point at the interface of two counterflowing layers can lead to the formation of a third layer of intermediate density. In these experiments where the halocline thickness was only a fraction of the shear-layer depth, the initial growth rate of the third or intermediate layer was constant and was independent of buoyancy effects. It is suggested that in this initial stage the growth rate is determined by the structure of the adjacent shear layer as discussed in §4.

The shape and ultimate extent of the intermediate layer was found to be sensitive to the buoyancy of the layers. If the stratification was strong, the intermediate layer tended to be long compared with its depth, and its final volume was limited by the extent of the sill. If the stratification was weak the intermediate layer was much thicker, and this could produce supercritical flow in the lower layer leading to the formation of an internal hydraulic jump. Active entrainment of fluid from the intermediate layer into the jump could lead to the eventual disappearance of the intermediate layer.

It is of interest to speculate on some naturally occurring flow in which intermediate layers might form by the convective mechanism described in this paper.

A fjord with a sill and a strong freshwater outflow may, during the period of tidal inflow, create a flow situation very similar to that examined in the experiments. Depths landward of the sill in a fjord are typically much greater than the depth of the halocline, so that velocities in the surface layer exceed those in the lower layer in this region. The point of velocity reversal is therefore located towards the very bottom of the halocline. However, at the sill during certain stages of the flood tide, it is well known that a two-layered counterflow can exist, with velocities in the lower layer exceeding the velocities in the upper layer. Such conditions would cause the stagnation line to rise, leading to the development of an intermediate layer in exactly the same manner as was demonstrated in the experiments.

Farmer & Smith (1980) have used high-frequency echo-sounding techniques to image internal structures in the vicinity of a sill in Knight Inlet, a fjord on the coast

FIGURE 11. Development of the intermediate layer in near-critical flow (experiment no. 9; $\Sigma F^2 = 0.61$, $Ri = 1.53$, $Re = 420$). (*a*) $\xi t = 102$; the interface has divided and the intermediate layer has commenced to form. Note the marked drawdown of the interface over the sill caused by the high value of ΣF^2 and interfacial disturbances resulting from the low value of Ri. (*b*) $\xi t = 150$; intermediate layer continuing to grow. The aspect ratio is much lower than was observed in the previously described experiments. (*c*) $\xi t = 210$; supercritical internal flow has developed in the lower layer to the right-hand side of the sill crest producing strong interfacial disturbances. (*d*) $\xi t = 320$; supercritical flow continues to develop in the lower layer and an internal hydraulic jump forms beneath the intermediate layer. Fluid from the intermediate layer is entrained into the jump and is convected away in the lower layer. (*e*) $\xi t = 516$; the intermediate layer has been completely engulfed by the internal jump. The internal jump is the dominant remaining feature of the flow.

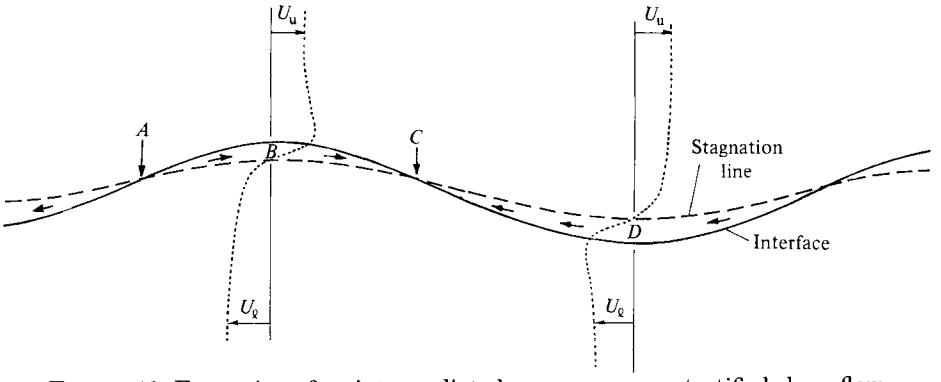

FIGURE 12. Formation of an intermediate layer on a wavy stratified shear flow.

of British Columbia. Echos from reflectors, which appear to associate with steep density gradients, show divisions of pycnoclines in a manner very similar to that described in this paper. Their figure 7 shows a flood tide entering as a subcritical bottom layer over the sill while the less dense surface layer continues to flow seawards. The division of the interfacial isopycnal at (*a*) and the existence of an apparent intermediate layer on the upstream side of the sill could be attributed to the convective mechanism.

Finally the mechanism may function in an internal wave field if certain conditions are satisfied. If internal waves exist at a sheared interface separating two layers of differing densities, and the mean velocities of the layers as seen by an observer moving with a wave are of nearly equal magnitude but of opposite sign, then the wave-induced velocity perturbations within the shear layer may produce convection towards a singular region on the interface. Such a flow field is shown in figure 12. The wave-induced perturbations to the simple shear flow increase velocities above a wave crest while reducing velocities beneath the crest. Thus fluid at the interface is driven by interfacial shear forces in the direction of flow in the upper layer as shown at *B* in figure 12. In the troughs (*D* in figure 12) the velocity perturbations are reversed so that interfacial fluid is convected in the direction of the lower layer. Thus fluid from the crest and the trough is convected towards a stagnation point on the forward face of the wave (*C* in figure 12). The formation of an intermediate layer by this process would depend on a shear layer of appropriate thickness developing over a distance of approximately one half-wavelength.

An experiment designed to simulate the formation of a mixed layer in a wavy shear flow was performed in the same experimental facility. The sill used in the earlier experiments was removed and inclined upper and lower boundaries were installed in the working section. The orientation of these boundaries was such that the velocity of each layer reduced in the direction of flow in either layer just as would be seen on the forward face of an internal wave by an observer travelling with the wave (figure 12). In these experiments a steady flow was established in the upper layer before starting the flow in the lower layer. Figure 13 shows the experiment at dimensionless time $\xi t = 140$ after commencement of the counterflow. As was observed in the previously described experiments, the interface divided and an intermediate layer began to develop. ΣF^2 in this experiment was equal to 0.56.

The authors wish to thank Professor J. S. Turner, Dr H. E. Huppert and a referee for helpful comments on the text of this paper.

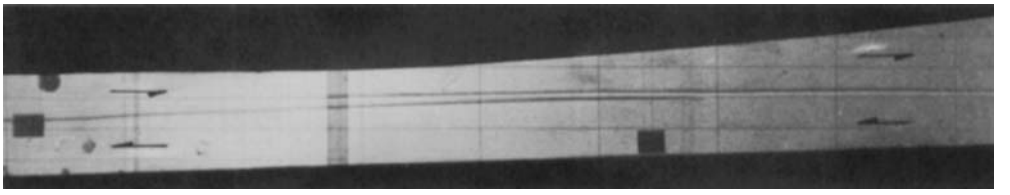

FIGURE 13. An intermediate layer formed between divergent shear layers such as might be produced by an internal wave at a sheared interface. F^2 in this experiment was equal to 0.56. The flow directions are indicated on the photograph, and the upper and lower boundaries have been retouched to improve clarity.

REFERENCES

FARMER, D. M. & SMITH, J. D. 1980 *Deep-Sea Res.* **27**A, 239–254.

MCEWAN, A. D. & ROBINSON, R. M. 1975 *J. Fluid Mech.* **67**, 667–687.

SHERMAN, F. S., IMBERGER, J. & CORCOS, G. M. 1978 *Ann. Rev. Fluid Mech.* **10**, 267–288.

TURNER, J. S. 1973 *Buoyancy Effects in Fluids.* Cambridge University Press.

WILKINSON, D. L. & WOOD, I. R. 1971 *J. Fluid Mech.* **47**, 241–256.